Reliability Analysis and Design Considerations for Exposed Column Base Plate Connections Subjected to Flexure and Axial Compression

Biao Song[1], Carmine Galasso[2], and Amit Kanvinde[3]

Abstract

Exposed Column Base Plate (ECBP) connections are commonly used in steel moment resisting frames. Current approaches for their design are well-established from a mechanistic standpoint. However, the reliability of connections designed as per these approaches is not as well understood. A detailed reliability analysis of the prevalent approach in the United States is performed in this study by using 59 design scenarios from steel moment frames subjected to combinations of dead, live, wind, and seismic loads. The analysis is conducted through Monte Carlo sampling reflecting uncertainties in the loads, material properties, component geometry, as well as demand and capacity models for the various components (base plate, footing, anchor rods) of the connection. Results indicate that the current design approach leads to unacceptable and inconsistent probabilities of failure across the various components. This is attributed to: (1) the use of a resistance factor for the footing bearing stress that artificially alters flexural demands on the base plate; and (2) the calibration of resistance factors for the plate and anchors without appropriate consideration of variability in demands. Two alternative approaches are examined as prospective refinements to the current approach. One eliminates the resistance factor for the bearing stress when used to determine flexural demands in the base plate, while the other considers overall failure of the connection, rather than failure of individual components within the connection. For both approaches, new resistance factors are calibrated to provide consistent and acceptable probabilities of failure across all limit states and all types of loading. Design and cost implications of these alternative approaches are summarized.

Keywords: Column Base Connections; Steel Connections; Reliability Analysis

[1] PhD Candidate, Department of Civil, Environmental & Geomatic Engineering, University College London, London WC1E 6BT, UK

[2] Associate Professor, Department of Civil, Environmental & Geomatic Engineering, University College London, London, WC1E 6BT, UK; and Scuola Universitaria Superiore (IUSS) Pavia, Pavia, 27100, Italy.

[3] Professor, Department of Civil and Environmental Engineering, University of California, Davis, CA, USA 95616; Corresponding author.

Introduction

Exposed Column Base Plate (ECBP) connections are widely used in low- to mid-rise Steel Moment Resisting Frames (SMRFs) to transfer forces from the entire structure, through the first-story column, into the concrete footing. Fig. 1 schematically illustrates an ECBP connection detail commonly used in the United States, and featured in design guidelines including the American Institute of Steel Construction's AISC *Design Guide One* (Fisher and Kloiber 2006), the Seismic Design Manual (AISC 2018), the AISC Specification (AISC 2016a), and the Seismic Provisions (AISC 2016b). Referring to the figure, the axial force and moment are transferred through a combination of upward bearing stresses (in the grout or supporting concrete) on the compression side of the connection, and downward tensile forces (in the anchor rods) on the tension side of the connection. Shear may be transferred either through friction (if sufficient compression is present), through the anchor rods, or through a shear key, if provided (Gomez et al. 2011). In the United States, the *Design Guide One* (abbreviated DG1 henceforth) is the primary document guiding the design of ECBP connections, under combinations of axial compression, flexure, and shear. The DG1 utilizes the internal stress distributions proposed by Drake and Elkin (1999). Connections that utilize similar details and force transfer mechanisms are used in other regions as well, e.g., Wald (2000) for Europe, and Cui et al. (2009) for Japan. Consequently, they have been studied extensively in various contexts. Ermopoulos and Stamatopoulos (1996) developed closed-form analytical solutions to characterize internal force distributions, and work by Gomez et al. (2010) and Kanvinde et al. (2013) has examined the efficacy of the DG1 method through experiments and finite element simulations, respectively. Other relevant work in the area includes Lee et al. (2008a; b) and Wald (2000) to examine various geometrical configurations and issues such as weld fracture which may occur under earthquake type cyclic loading (e.g., see Fahmy 2000; Myers et al. 2009). More recently, the focus has shifted to the seismic performance of these connections, to investigate their possible use as dissipative fuses (e.g., Falborski et al. 2020; Trautner et al. 2016).

These studies concur that the Drake and Elkin (1999) approach (which underlies the *de facto* design method in the United States through DG1) is effective from a mechanistic standpoint, i.e., it is able to satisfactorily characterize the internal force distribution within ECBP connections in a deterministic sense (Gomez et al. 2010; Kanvinde et al. 2013). However, a closer examination of the method (and associated literature) from a probabilistic standpoint (e.g., Aviram et al. 2010) reveals inconsistencies that must be addressed to ensure that ECBP connections meet target reliability (i.e., provide acceptable probabilities of failure/safety levels). These issues emerge because the approach treats the ECBP connection as a collection of components, each designed separately, without considering their collective effect on the connection failure. Specifically, the approach determines an internal force distribution (i.e., forces in the anchor rods, and bending moments in the base plate) based on an assumed bearing stress distribution in the concrete/grout, and then applies design checks independently to each of these components (i.e., the anchor rods and base plate) by comparing these estimated forces/moments to their capacities, modified by resistance (i.e., $\phi-$) factors. This is problematic for numerous reasons:

- Connection failure is controlled by interactions of these components. Research by Gomez et al. (2010), as well as Kanvinde et al. (2015), has indicated that flexural yielding of the base plate on the compression side of the connection does not result in connection failure, unless also accompanied either by yielding of the anchor rods, or by flexural yielding of the base plate on the tension side. Applying design checks independently to these components disregards this effect, resulting in undue conservatism.
- From the perspective of system reliability, applying the design checks independently is inappropriate, because the probability of failing one design check may not necessarily

correspond to failure of the entire connection.

- The assumed bearing stress in the concrete (used for determination of the internal force distribution) includes a $\phi-$factor to incorporate the uncertainty in this stress. While this may be suitable for design of the concrete footing itself (to provide a conservative estimate of bearing stress), it cannot be justified for design of the other components (i.e., base plate and anchor rods). This is because the bearing stress effectively acts as a "demand" on these other components through overall equilibrium of the connection, such as that a lower estimate of bearing stress may, in fact, be unconservative.
- Finally, the $\phi-$factors in the independent design checks for the anchor rods and base plates are borrowed in an *ad hoc* manner from other similar components, and are not based on reliability analysis. Specifically, the design checks consider only the uncertainty in capacities of the components and disregard both the uncertainty as well as bias in the estimated forces and moments in these components.

Other researchers have also noted that the DG1 approach does not incorporate reliability analysis. Torres-Rodas et al. (2020) performed reliability analysis for the DG1 approach, with a primary focus on uncertainty in seismic demands. Their analysis addresses the overall response of the connection, and does not consider the interaction of various components. Nonetheless, the results indicate that the reliability provided by the DG1 approach is unacceptable. In summary: (1) while well-intentioned, the DG1 approach fails to effectively incorporate system reliability as well as overall connection response; and (2) given the complex and sometimes counteracting nature of the effects noted above, consistent connection reliability cannot be ensured. In response to these issues, this study conducts a detailed analysis of the current DG1 approach for the design of ECBP connections, with the following objectives:

1. To examine the level of connection reliability (conventionally quantified by the reliability index β) provided by ECBP connections designed as per the DG1 approach, with a focus on its consistency across various design scenarios as well as component failure modes.
2. To identify deficiencies in the DG1 approach and examine possible enhancements that are based on considering system response, and eliminating the use of $\phi-$ factors that do not comport with physics.
3. Based on these analyses, to suggest prospective design strategies that ensure acceptable and consistent performance/reliability, while also incorporating overall connection behavior.

The paper begins by providing background, including the DG1 approach; this is followed by a summary of the methodology used for reliability analysis. A set of 59 design scenarios (SMRF columns for which ECBP connections must be designed) that represent various combinations of gravity, wind, and seismic loading are then described. For each of these scenarios, ECBP connections are designed using existing as well as proposed approaches, and reliability analyses are conducted using Monte Carlo simulations modelling several sources of uncertainty. The paper concludes by providing commentary regarding the analyzed approaches and suggesting strategies that ensure consistent reliability.

Background and Review of Current Design Practice

Fig. 2 illustrates the key assumptions of the DG1 method. Note that the superscript (i.e., DG1) of some symbols in the figure indicates the design method used to determine the internal forces and moments in the ECBP connection. Since this method is well documented in the design guide itself, it is only briefly summarized here. Referring to Fig. 2, the axial compression (P) and moment (M)

combination is resisted by: (1) a compression stress block of constant magnitude (= f), if the axial force is high relative to moment, i.e., a "low-eccentricity" condition; or (2) a compression stress block (of magnitude = $f_{\text{max}}^{\text{DG1}}$) supplemented by tension ($T_{\text{rods}}^{\text{DG1}}$) that develops in the anchor rods as the base plate uplifts when the axial compression is low compared to the moment, i.e., a "high-eccentricity" condition. The process for design involves the following steps:

- Determine whether the condition is low-, or high-eccentricity. For this, the critical value of load eccentricity (e_{crit}) is determined as:

$$e_{crit} = \frac{N}{2} - \frac{P}{2 \cdot B \cdot f_{\text{max}}^{\text{DG1}}} \tag{1}$$

  The terms B and N denote the length and width of base plate. The above assumes that the bearing side of the connection develops a rectangular stress block with a constant magnitude $f_{\text{max}}^{\text{DG1}}$, determined as $\phi_{\text{bearing}} \times \min\,(f_{\text{grout}}, f_{\text{concrete}})$, where the ϕ_{bearing} – factor is taken as 0.65, f_{grout} is the crushing strength of the grout, whereas f_{concrete} is estimated as below, accounting for the effects of concrete confinement (if the footing is larger than the base plate):

$$f_{\text{concrete}} = 0.85 \cdot f_c^{'} \cdot \sqrt{\frac{A_2}{A_1}} \leq 1.7 \cdot f_c^{'} \tag{2}$$

  In the above equation, $f_c^{'}$ is the compressive strength of the concrete, A_1 is the bearing area of the plate, and A_2 is the effective area of the concrete (typically the plan area of the footing). The grout pad is usually not confined similarly, since it is above the concrete surface. Thus, a similar adjustment is not required for the grout strength (f_{grout}).

- For low-eccentricity, i.e., the design load eccentricity e (= M/P) < e_{crit}, the magnitude of the upward bearing stresses f, as well as the stress block length Y^{DG1} (Fig. 2(a)) may be readily calculated through force and moment equilibrium. If a suitable equilibrium solution cannot be found with $f < f_{\max}^{\mathrm{DG1}}$ and $Y^{\mathrm{DG1}} < N$, then the base plate plan dimensions must be resized – the concrete/grout bearing failure check is applied implicitly in this manner. This design check is denoted *BF* (representing the Bearing Failure limit state) to facilitate subsequent discussion of the reliability analysis. For the low-eccentricity condition, the only other possible mode of failure is flexural yielding of the base plate on the compression side due to bearing stresses; this is calculated by assuming that the toe of the base plate bends upwards as a cantilever flap, with a yield line parallel to the edge of the column compression flange. This design check is denoted *PC* (Plate failure on the Compression side). Specifically, failure is assumed to occur if the cantilever moment (denoted $M_{pl,comp}^{\mathrm{DG1}}$) over the yield line exceeds the reliable capacity of the base plate, i.e., $\phi_{\mathrm{plate}} \times M_p^{\mathrm{plate}}$, where $M_p^{\mathrm{plate}} (= F_{y,pl} \cdot B \cdot t_p^2 / 4$, $F_{y,pl}$ is the yield strength of base plate steel and t_p is the thickness of base plate) refers to the plastic moment capacity of the base plate, and $\phi_{\mathrm{plate}} = 0.9$.

- If $e \geq e_{crit}$, i.e. the "high-eccentricity" condition (Fig. 2(b)), then the stress in the bearing zone reaches its maximum value (i.e., $f_{\max}^{\mathrm{DG1}}$), such that the two remaining unknowns, i.e., the stress block length Y^{DG1} as well as the tension forces in the anchor rods $T_{\mathrm{rods}}^{\mathrm{DG1}}$ may be calculated from force and moment equilibrium, as per the following equations:

$$Y^{\mathrm{DG1}} = (N-g) - \sqrt{(N-g)^2 - \frac{2 \cdot \left[M + P \cdot \left(\frac{N}{2} - g \right) \right]}{f_{\max}^{\mathrm{DG1}} \cdot B}} \tag{3}$$

$$T_{\text{rods}}^{\text{DG1}} = f_{\max}^{\text{DG1}} \cdot B \cdot \left(\left(N-g\right) - \sqrt{\left(N-g\right)^2 - \frac{2 \cdot \left[M + P \cdot \left(\frac{N}{2} - g \right) \right]}{f_{\max}^{\text{DG1}} \cdot B}} \right) - P \tag{4}$$

This results in four possible limit states, and associated design checks. As in the low-eccentricity case, the *BF* design check is applied implicitly, such that failure is assumed to occur if $Y^{\text{DG1}} > N - g$ (where g is the distance between the center of the anchor rods to the edge of the base plate, see Fig. 2(b)), which indicates that the bearing zone extends into the tension anchor rods (which is impossible from a compatibility standpoint). For the base plate, two limit states are possible: (1) the *PC* limit state due to upward bearing on the compression side; and (2) flexural yielding of the base plate on the tension side due to downward tension forces in the anchor rods; this is denoted *PT*, and evaluated by comparing the moment in the plate due to the anchor forces $T_{\text{rods}}^{\text{DG1}}$ (denoted $M_{pl,ten}^{\text{DG1}}$) and the reliable capacity $\phi_{\text{plate}} \times M_p^{\text{plate}}$. For the *PT* limit state, the controlling mechanism may involve either a yield line parallel to the column flange or inclined to the plate edge, depending on the location of the anchor rods. The final limit state is the yielding of the anchor rods themselves, which is determined to occur if $T_{\text{rods}}^{\text{DG1}}/n_{\text{rod}} > \phi_{\text{rod}} \times 0.75 \cdot F_u^{\text{rod}} \cdot A_{\text{rod}}$ (where n_{rod} is the number of anchor rods in a line, F_u^{rod} is the ultimate strength of the rod, A_{rod} is the unthreaded area of anchor rod, and $\phi_{\text{rod}} = 0.75$) – this is denoted *AT*. Other anchor limit states include rod pullout or concrete blowout. These depend on the footing configuration and reinforcement, and are outside the scope of this article; American Concrete Institute (ACI) 318 (ACI 2019) provides greater detail.

Each of the design checks outlined above includes $f_{\max}^{\text{DG1}}$, and consequently ϕ_{bearing}, which is used to estimate it. For the *PC* check, the non-conservatism is readily apparent because ϕ_{bearing} reduces the bearing stress, which acts as a "load" on the cantilever flap for the *PC* limit state. The effect of ϕ_{bearing} on the other limit states is not as direct (see Eqs. (3) and (4)). Nonetheless, it is evident that for the same reasons as for the *PC* check, incorporating ϕ_{bearing} within the design checks is not appropriate, and is likely to result in biased or inaccurate characterizations of reliability. Finally, as discussed earlier, the ϕ_{plate} and ϕ_{rod} do not consider either the accuracy of the demand estimation within the individual components or the variability within it – which is also inappropriate from the perspective of estimating reliability. The next section outlines a process for estimating the reliability of ECBP connections that addresses these various issues, before applying it to the current and prospective design approaches.

Methodology for Reliability Assessment of ECBP Connections

This section describes the process of evaluating the reliability of ECBP connections for which the nominal configuration (i.e., geometry, material properties), as well as the design loadings are known. Once this process is established for a given connection, it may be used to test alternative strategies resulting in specific designs. The main steps involved in this process (see Fig. 3) are:

- Developing a set of representative and realistic loading scenarios, in terms of the applied moment (*M*) and axial forces (*P*) combinations at column bases for which ECBP connections are to be designed.
- Designing the ECBP connections as per the appropriate design method (DG1 or prospective), sometimes resulting in multiple configurations, each of which satisfy all design checks.
- Identifying sources of uncertainty in each designed configuration.

- For each configuration, formulating limit-state functions associated with each failure mode, i.e., *BF*, *PC*, *PT*, and *AT*.
- Performing Monte-Carlo sampling that utilize the statistical distributions of input random variables (RVs) to assess the probability of failure (P_f) and reliability indices (β) of each designed configuration.

Generation of Representative Design Cases

The design condition for ECBP connections is defined by a combination of moment (M) and axial force (P); shear is not considered in this study and is assumed to be transferred independently, e.g., through a shear key – see Gomez et al. (2011). To ensure realism in these P-M load pairs, these are not arbitrarily generated, but derived from four archetype steel moment frames (each consisting of four stories and three bays). These designs, based on ASCE 7-05 (ASCE 2006) and AISC 341-05 (AISC 2005), are selected from an archetype set of special steel moment frames developed by the National Earthquake Hazards Reduction Program (NEHRP 2010); only key details are provided here. Table 1 summarizes the member properties, whereas Fig. 4 illustrates the dimensions and floorplans. The key differences between the frames are the level of seismicity they are designed for (also indicated in Table 1, in accordance with Seismic Design Category, SDC, i.e., SDC-D_{max} or SDC-D_{min}) and the method used to design them (Response Spectrum Analysis, RSA; or the Equivalent Lateral Force, ELF). Four-story frames are selected for the representative load case, because taller frames usually warrant embedded base connections (e.g., see Grilli et al. 2017), whereas 1-2 story frames often assume ECBP connections to be pinned (e.g., see Zareian and Kanvinde 2013).

For each frame, Dead (D), Live (L), and Earthquake (E) loads are determined from the applicable code used in the frame design, i.e., ASCE 7-05 (ASCE 2006). Wind (W) load was not considered in the original frame design, and it is determined as per ASCE 7-16 (ASCE 2016). Corresponding P and M values at each of the column base locations in each building are recovered, and subsequently used to generate P-M pairs based on the load combinations indicated in Table 2. These load combinations include those prescribed by ASCE 7-16, as well as others that are informed by recent research and other standard practices. For example, Torres-Rodas et al. (2018) indicate that the minimum (rather than maximum) compressive axial force in the column may control the design of some ECBP connections, since lower compression increases tension in the rods. The load factor $-\Omega_0 E$ (in which Ω_0 represents the "overstrength" seismic load) reflects the overturning effect that minimizes axial compression. The factor $1.1R_yM_p$ in some of the seismic load cases reflects a capacity design (AISC 341-16 2016b), which is often specified in high-seismic zones to induce a plastic hinge the attached column, rather than in the connection. Referring to Table 2, the exterior and interior base connections within each frame are designed separately. This results in the generation of five P-M pairs for which each ECBP connection must be designed – two pairs of seismic and two pairs of wind load combinations, considering maximum or minimum P associated with its M, in addition to a P-M pair derived from the gravity load combination.

Once the P-M pairs are generated as above, the ECBP connections may be designed as per any approach (e.g., the DG1 approach or prospective approaches) with the following additional information/material specifications that are representative of standard practice: (1) nominal concrete compressive strength $f_c^{'}$ = 27.58 MPa (4 ksi), and f_{grout} = 58.61 MPa (8.5 ksi); (2) concrete confinement factor (i.e., $\sqrt{A_2/A_1}$) assumed to be equal to its maximum value of 2.0; (3) ASTM A992 ($F_{y,col}$ = 345 MPa) steel used for all the beams and columns; (4) base plate material specified as A572 (Grade 50, $F_{y,pl}$ = 345 MPa); (5) anchor rod material selected from two available grades of ASTM F1554 steel, i.e., Grade 55 (F_u = 517 MPa), Grade 105 (F_u = 862 MPa); (5) a minimum of four anchor rods (with diameters d_{rod} in the range of 19.05 – 63.5 mm) provided as per Occupational Safety and Health Administration requirements (OSHA 2001), and 76.2 mm (3 in) edge distances (g) used for all anchor holes following standard practice; (6) base plate thicknesses (t_p) varied in 3.18 mm (1/8 in) increments up to 31.75 mm (1¼ in) thickness and in 6.35 mm (1/4 in) above this; (7) in-plane dimensions of base plate (N and B) varied in 50.4 mm (2 in) increments, and assumed to be identical for different design approaches. In addition, three examples available in the design manuals (i.e., two from DG1 and one from the design manual of Structural Engineers Association of California, SEAOC 2015) are also analyzed in this study, since these represent the only published guidance for ECBP connection design. Note that the base plate material (A36, $F_{y,pl}$ = 248 MPa), anchor rod material (ASTM F1554 Grade 36, F_u = 400 MPa) used in these DG1 examples are representative of erstwhile construction practice, and different from those used in this study. The details of all the 59 P-M cases (for design) are further summarized in Table 2.

Characterization of Uncertainty

Using the above considerations, and the appropriate set of design checks (DG1 or the ones proposed later in this article), ECBP connections may be designed. This results in the selection of the following design variables: (1) Geometric parameters: overall depth (d), flange width (b_f), flange thickness (t_f) and web thickness (t_w) of base column section (W-shape), length (N), width (B) and thickness (t_p) of base plate, diameter (d_{rod}) of anchor rods, and edge distance (g) of anchor holes; and (2) Material parameters: concrete compressive strength ($f_c^{'}$), grout strength (f_{grout}), yield strength of base column ($F_{y,col}$) and base plate ($F_{y,pl}$) steels, as well as the tensile (ultimate) strength of anchor rods (F_u). Once this has been accomplished, reliability assessment of each designed ECBP connection requires the characterization of uncertainty arising from four sources: (1) geometry of each component; (2) material properties; (3) applied loads on the connection; and (4) mechanical models used to characterize the demand and capacity of each component. Table 3 summarizes the uncertainties used for Monte Carlo sampling (discussed later). These are represented as RVs with statistical distributions that reflect the bias coefficient (i.e., the ratio between the mean value of each RV to its nominal value as specified in the design cases mentioned above), and the coefficient of variation (CoV, defined as the ratio between the standard deviation of each RV to its mean value). All these RVs are considered statistically independent.

Component Geometry

Uncertainty in component geometry is attributable to construction or fabrication processes, tolerances, and the resulting quality (Nowak and Szerszen 2003). Dimensional statistics of W-shape column sections are collected from Schmidt and Bartlett (2002); these include the overall depth (d), flange width (b_f), flange thickness (t_f) and web thickness (t_w) – note that the these are relevant for calculating $1.1R_yM_p$ (for capacity design) as well as for determining edge distances/cantilever lengths for plate flexure limit states. According to Aviram et al. (2010), the standard deviations of base plate dimensions (i.e., length N, width B and thickness t_p) and anchor rod diameter (d_{rod}) are established based on their tolerances specified in ASTM A6-19 (2019) and ASTM F1554-18 (2018), respectively. The tolerance (standard deviation) of edge distance (g) is defined as per AISC 303-16 (2016c). The bias factors are assumed equal to 1.0 to represent average quality of construction or fabrication. Moreover, the normal distribution is assumed for these dimensional RVs with a relatively small CoV (i.e., < 10%), as expected for geometry-related RVs.

Material Properties

The statistical properties of concrete compression strength for nominal $f_c^{'}$ = 27.58 MPa (4 ksi) are comprehensively documented in Nowak and Szerszen (2003), in which 116 concrete samples obtained from different concrete industrial sources in the United States were assessed. According to testing by Gomez (2010), the compressive strength of grout (f_{grout}) is 58.61 MPa with a CoV of 13%. Statistics of structural steel used for the column and base plate were assembled from a detailed survey by Liu et al. (2007). These properties include the yield strength ($F_{y,pl}$) of base plate materials (both ASTM A572 Grade 50 and ASTM A36 steels), and the yield stress ($F_{y,col}$) of the A992 steel used for the base columns. Statistical distributions for the anchor rod tensile strength (F_u) of ASTM F1554 steels are characterized based on the approach of Aviram et al. (2010) and the tolerances given in ASTM F1554-18 (2018). Table 3 summarizes the distributions as well as statistical parameters for all material properties.

Applied Loads

Combinations of Dead (D), Live (L), Earthquake (E), and Wind (W) loads are considered to determine the axial (P) and flexural (M) forces acting on the ECBP connections. The RV describing the dead load is usually assumed as normally distributed and Ellingwood et al. (1980) suggests a bias of 1.05 and a CoV of 10%. For the RVs to describe live load and wind load, a Gumbel-type distribution is selected (Ellingwood et al. 1980), and their bias and CoV values are summarized in Table 3. For the earthquake load, a lognormal distribution with a bias of 1.0 is assumed, based on the calibration by Fayaz and Zareian (2019) using linear time-history analysis. The assumed bias is also close to the value suggested by Ellingwood et al. (1980) for a site in Los Angeles, CA. It is also worth noting that Torres-Rodas et al. (2018) performed nonlinear time-history analyses to characterize demands in ECBP connections in 4-story steel moment frame (similar to one of the selected frames in this study). Their findings indicate bias values of 1.17 and 1.02 for the determination of axial force (for interior and exterior column bases, respectively) subjected to the seismic load combination (i.e., $P = 1.2D + 0.5L + \Omega_0 E$). A CoV of 60% is arbitrarily assumed here for the distribution of the maximum earthquake load effects over a service period of 50 years. It is worth highlighting that an explicit/advanced calibration of the earthquake-induced demands (and their distributions) for each case-study connection and the consequent seismic reliability assessment would require performing nonlinear time-history analyses using hazard-consistent ground motions (for a given target site) and integrating the obtained structural demands with a site-specific hazard curve, as done for instance in Torres-Rodas et al. (2020) (or similarly in Fayaz and Zareian (2019) by using linear time-history analysis). This is outside the scope of this study. The simplified approach used here is deemed appropriate to compare and discuss different design strategies for ECBP connection as proposed in this paper. Note that for the cases that involve capacity-design for calculation of the moment (i.e., $M = 1.1R_yM_p$, nominally, where, $M_p = F_{y,col}Z_x$ where Z_x is the plastic modulus of the section), the uncertainty in geometry and material properties (outlined in the previous subsections) is used to simulate uncertainty in $1.1R_yF_{y,col}Z_x$. Referring to Table 3, the bias factor as well as the distribution for $F_{y,col}$ includes the R_y effect (i.e., the difference between specified and true yield stress), based on Liu et al. (2007).

Mechanical Models

Model uncertainties, often known as professional uncertainties, connote the error in demand or capacity estimates determined through models or equations. In general, these may be determined by comparing the demand or capacity obtained in experimental or numerical tests with the corresponding values obtained via analytical formulations or simplified models. On the capacity side, the expressions for plate bending strength (i.e., $M_p^{\text{plate}} = F_{y,pl} \cdot t_p^2/4$) as well as the anchor rod strength (i.e., $T_R^{\text{rods}} = n_{\text{rod}} \cdot 0.75 \cdot F_u^{\text{rod}} \cdot A_{\text{rod}}$) are derived from basic mechanics and are straightforward; consequently errors in their estimations are assumed to be negligible and not considered in this study. The bearing stress of the concrete/grout ($f_{\max}$) includes the factor $0.85 \cdot \sqrt{A_2/A_1}$ (to reflect the confining effect of the concrete footing – refer Eq. (2)), and may be expressed in the following manner:

$$f_{\max} = \min\left(f_{\text{grout}}, \frac{f_{\text{concrete}}^{\text{test}}}{f_{\text{concrete}}^{\text{Eq.(2)}}} \times \left(0.85 \times f_c^{'} \times \sqrt{\frac{A_2}{A_1}} \right) \right) \tag{5}$$

Expressing the bearing stress of concrete in this manner allows for the incorporation of model uncertainty through the term $f_{\text{concrete}}^{\text{test}} / f_{\text{concrete}}^{\text{Eq.(2)}}$ in Eq. (5), which may be simulated as an RV. Comparison of experimental data by Hawkins (1968), for $f_{\text{concrete}}^{\text{test}}$, to the solutions obtained by Eq. (2) ($f_{\text{concrete}}^{\text{Eq.(2)}}$) is used to determine the parameters for the distribution of error in bearing stress calculation – see Table 3. On the demand side, the primary modeling uncertainties are in the estimations of bending moments on the compression side and tension side of base plate (denoted as $M_{pl,comp}$ and $M_{pl,ten}$, respectively), as well as tension forces in the anchor rods (T_{rods}). These uncertainties arise from the simplifying assumptions of the strength characterization method itself (i.e., the rectangular stress block, and arising internal force distribution). For the tensile force demands in the anchor rods, experimental data from Gomez et al. (2010) as well as Kanvinde et al. (2015) are informative because these feature direct measurement of anchor rod forces through strain gages or load cells. These findings are supplemented by Continuum Finite Element (CFE) by Kanvinde et al. (2013). Based on these results, the model uncertainty in the estimated anchor rod forces may be represented through an RV ($T_{\text{rods}}^{\text{true}} / T_{\text{rods}}^{\text{model}}$, see Table 3):

$$T_{\text{rods}} = \left(\frac{T_{\text{rods}}^{\text{true}}}{T_{\text{rods}}^{\text{model}}} \right) \cdot T_{\text{rods}}^{\text{model}} \tag{6}$$

The two other quantities, i.e., $M_{pl,comp}$ and $M_{pl,ten}$, are challenging to measure experimentally; consequently, their CFE-based estimates (from Kanvinde et al. 2013) are used to characterize model uncertainty in them through the RVs, $M_{pl,comp}^{\text{true}} \big/ M_{pl,comp}^{\text{model}}$ and $M_{pl,ten}^{\text{true}} \big/ M_{pl,ten}^{\text{model}}$ (whose distributions are also summarized in Table 3). These may be expressed as:

$$M_{pl,comp} = \left(\frac{M_{pl,comp}^{\text{true}}}{M_{pl,comp}^{\text{model}}} \right) \cdot M_{pl,comp}^{\text{model}} \tag{7}$$

$$M_{pl,ten} = \left(\frac{M_{pl,ten}^{\text{true}}}{M_{pl,ten}^{\text{model}}} \right) \cdot M_{pl,ten}^{\text{model}} \tag{8}$$

Note that in the above equations, the superscript "model" is used to denote a model generically and may be used for the DG1 model or those suggested herein; these result in distinct distributions – each determined by comparing estimates from the corresponding model to the CFE or test results (indicated by the superscript "true").

Formulation of Limit States

As discussed in the previous section, four failure modes of ECBP connections subjected to combined flexural and axial loadings have been identified: (1) bearing failure in the footing – *BF*; (2) flexural yielding of base plate on the compression side – *PC*; (3) flexural yielding of base plate on the tension side – *PT*; and (4) anchor rod yielding – *AT*. For each of these, conditions that lead to failure may be expressed as limit-state functions (G) defined as the difference between the capacity (C) and counterpart demand (D):

$$G = C - D \tag{9}$$

Failure of each component occurs when demand exceeds capacity, i.e., $G < 0$. Following this, the limit-state functions of three of the four individual failure modes (i.e., *PC*, *PT*, *AT*) may be formulated as below:

$$G_{PC} = C_{PC} - D_{PC} = M_p^{\text{plate}} - M_{pl,comp} \quad (10)$$

$$G_{PT} = C_{PT} - D_{PT} = M_p^{\text{plate}} - M_{pl,ten} \quad (11)$$

$$G_{AT} = C_{AT} - D_{AT} = T_R^{\text{rods}} - T_{\text{rods}} \quad (12)$$

All the terms in Eqs. (10)-(12) are discussed above, in the Mechanical Models subsection. For the *BF* failure mode, the limit-state function cannot be formulated in a single equation because failure is assumed to occur when the bearing stress f and bearing width Y required to resist the applied P-M combination, violates either of the following conditions:

$$f < f_{\max} \quad (13)$$

$$Y < N - g \quad (14)$$

The former (Eq. (13)) enforces the condition that the maximum stress is limited by the bearing capacity of the grout/concrete footing, whereas the latter (Eq. (14)) disallows the unphysical development of a zone of compression in the foundation under the tensile anchor rods.

Monte Carlo Sampling and Reliability Assessment

For each of the design cases, plain Monte Carlo sampling is used to simulate the demands (D) and capacities (C) of each failure mode described above. The Monte Carlo sampling is conducted through a MATLAB code developed by the authors, and used to estimate the probability of the limit-state functions (as formulated above) being negative, i.e., the probability of failure (P_f):

$$P_f = \Pr(G < 0) = \Pr(C - D < 0) \quad (15)$$

A total of 10^8 samples (of the RV sets with statistics listed in Table 3) are randomly generated, and the P_f of each failure mode is estimated through a one-by-one check of G in each simulation:

$$P_f = \frac{\text{Number of } G < 0}{\text{Total Number of Samples } \left(=10^8\right)} \tag{16}$$

Then, a commonly-used measure of reliability, known as the reliability index β (Cornell 1969), is adopted to evaluate the results. If G follows a normal distribution, β is related to P_f via the standard normal cumulative distribution function Φ:

$$P_f = \Phi(-\beta) \Leftrightarrow \beta = -\Phi^{-1}\left(P_f\right) \tag{17}$$

Even though G does not have a normal distribution it is common practice to convert the failure probabilities to β through Eq. (17) as an indicator of reliability; the approximation associated with this conversion is usually very low (Iervolino and Galasso 2012). For each simulation, a total 10^8 samples are used; this sample size of Monte Carlo simulation is able to achieve stable estimates of a $P_f = 3.17\times10^{-5}$ (corresponding to a target reliability index, $\beta_T = 4.0$) with a CoV of 2% or less (Nowak and Collins 2012).

Acceptable or "target" β_T values for a given component usually depend on the consequences of component failure on system performance, because the ultimate goal is to limit the annual probability of system collapse to a tolerable level (Victorsson 2011). However, tuning the probability of failure of each component within a system to achieve a target annual probability of system failure is typically infeasible due to the multitude of variables and uncertainties involved in the process. As a result, the LRFD approach (also used in the DG1) sets lower target probabilities of failure for connections (whose failure is assumed to be catastrophic) compared to members. Specifically, the target probability of connection failure is set at 2.5 orders of magnitude lower than member failure. This is reflected in the target reliability indices of 4.5 and 3.0 for connections and members (under dead and live loadings), respectively (AISC 1986). Similarly, $\beta_T = 4.1$ (for dead plus live plus wind loading, i.e., wind load combination) and 3.6 (for dead plus live plus earthquake loading, i.e., seismic load combination) are recommended for connection design. Following this rationale, these target β_T values (4.5 for gravity, 4.1 for gravity and wind, 3.6 for gravity and seismic) are adopted in this study.

This above reliability assessment process is first applied to the designs generated by the ECBP connections designed as per the DG1; this is the topic of the next section. Based on the results of this reliability assessment, refinements to the approach are proposed, and the reliability assessment process is reapplied to connections designed with these refinements.

Reliability Analysis of ECBP Connections Designed as per Current Practice

The methodology discussed in the previous section is applied to analyze the structural reliability of 59 ECBP connections designed as per current practice, i.e., the DG1 method. For all these connections, a β value (reflecting the probability of failure) is computed for each of the four failure modes. These β values are represented as histograms in Fig. 5. Specifically, Fig. 5 shows the median β value (with error bars representing lower and upper quartiles, i.e., 25th and 75th percentiles) for various subsets of data to examine reliability with respect to different failure modes and under different loadings. The histograms in Fig. 5 are grouped into sets, each corresponding to a failure mode (i.e., *BF*, *PC*, *PT* and *AT*). Within each set, the three bars correspond to different loading combinations, i.e., gravity only, gravity plus wind loading, and gravity plus earthquake loading. Referring to Fig. 5, the following observations may be made:

- The median β value for the *PC* limit state (i.e., flexural yielding of the plate on the compression side) is the lowest compared to the other failure modes, indicating the highest probability of failure. The range of these β values (1.1 – 2.3, with a median of 1.5) corresponding to the seismic load combinations (designed mainly for high-eccentricity conditions) is unacceptable relative to conventional expectations of reliability for connections (that require a β value of 3.6), as outlined earlier. This non-conservatism is not surprising, considering the use of the ϕ_{bearing} – factor (discussed earlier) within the bearing stress block, which artificially decreases the flexural demand on the base plate on the compression side of the connection. While this is problematic from a reliability standpoint, experimental research by Gomez et al. (2010) and Kanvinde et al. (2015) indicates that exceeding this limit state (i.e., base plate yielding on the compression side) may not result in loss of strength – owing to the high ductility associated with this mechanism. A total of 15 experiments in these studies indicate that the connection continues to gain strength even after the *PC* limit state, reaching its capacity only when a limit state on the tension side (i.e., either *PT* or *AT* limit state) is also attained. Based on this information, the Seismic Provisions (AISC 341-16 2016b, Commentary) suggest that the ultimate strength of the ECBP connection be calculated upon attainment of yielding on both the tension and compression sides of the base plate.

- For the *PT* and *BF* limit states, satisfactory reliability (median β > 4.0) is achieved across all loading cases. In fact, in many of these cases, the histograms are shown as incomplete because no failure was observed in the 10^8 RV realizations for the Monte Carlo sampling.

- For the *AT* limit state, the reliability for the design cases corresponding to seismic load is unacceptable (median β value of 1.7), while it is acceptable for the other loading cases.

- Fig. 5 also indicates a reliability index corresponding to "connection failure", which corresponds to the weakest failure mode (i.e., the lowest β) in each of the design cases – this is shown as a separate group of histograms. Referring to these, the β values for most of the load cases (46 out of 59 cases) are identical to those for the *PC* limit states. A closer examination of the data indicates that for these design cases, the *PC* limit state has the lowest reliability, while the *AT* and *PT* limit states are observed as the weakest failure mode for the 11 and two exceptions, respectively.

- For all limit states, it is noted that the β value associated with the seismic load cases is significantly lower than that associated with the other (gravity and wind) load cases, and also unacceptable relative to the values outlined above for *PC* and *AT* limit states (with median β of 1.5 and 1.7, respectively).

In summary, the reliabilities attained for ECBP connections designed as per the DG1 approach are inconsistent across various limit states as well as loadings. For a few of these limit states and loading cases, the reliability estimates are clearly unacceptable.

Alternative Design Approaches

The above discussion motivates alternative design approaches that mitigate the problems of the DG1 approach. It is evident that the use of the $\phi_{\mathrm{bearing}}-$factor in the determination of plate bending moments and anchor rod forces is problematic from both a mechanistic and a reliability standpoint. Further, it is noted that *PC* limit state is the most critical in terms of reliability, although exceedance of this limit state does not result in overall failure of the connection, as suggested by AISC 341-16 (AISC 2016b). Following these observations, two alternative design approaches are considered:

- The first approach (termed DG1*) is identical to the DG1 approach, except for the omission of the $\phi_{\mathrm{bearing}}-$factor in the determination of the anchor rod tension as well as the plate flexural stresses. All limit states, i.e., *BF*, *PC*, *PT*, and *AT* are checked in design.

- The second approach (termed CF – Connection Failure) is similar to DG1*, i.e., the $\phi_{\text{bearing}} -$ factor is not considered. However, only the *PT* and *AT* limit states are checked, assuming that overall failure of the connection does not occur at until at least one of these is attained.

In each of these approaches, the plan dimensions of the base plate are designed as per DG1i.e., using ϕ_{bearing} = 0.65 to check the *BF* limit state (see Table 2), as discussed earlier, therefore, the results of *BF* check are identical to those in the previous sections. It is emphasized here that the use of ϕ_{bearing} = 0.65 is problematic only when the bearing stress is being considered a demand or loading on the remainder of the base connection. Using both approaches, ECBP connections are re-designed for each of the loading cases summarized previously in Table 2 (and also used for generation of designs for the reliability analysis of the DG1 approach). Within each of these approaches, a range of trial $\phi-$ factors are used to size both the plate (using ϕ_{plate} = 0.9, 0.8, 0.7, 0.6, 0.5 and 0.4) and the rods (using ϕ_{rod} = 0.75, 0.65, 0.55, 0.45 and 0.35). This enables effective selection of $\phi-$ factors that provide adequate safety for all limit states and loading scenarios. The resulting design configurations (i.e., base plate and anchor rod sizes) may then be subjected to reliability analysis in a manner similar to that conducted for the DG1 approach. Specifically, the Monte Carlo sampling follows exactly the same procedure as earlier (for DG1), with uncertainties characterized through the RVs and their distributions summarized in Table 3. The key results of these simulations are the probabilities of failure, expressed in terms of equivalent β factors for various limit states and design cases.

Figs. 6(a)-(e) plot the β values versus the corresponding $\phi-$ factors for the DG1* approach. The clusters of β for each value of $\phi-$ factor represent the different ECBP designs that all satisfy the design checks; the graph line connects the median β values of these clusters. Referring to these figures, the *BF* limit state is not included in these graphs because only a single ϕ_{bearing} – factor (i.e., 0.65) is used for sizing the footprint (i.e., plan dimensions) of the base plate. Further, the tension side limit states (*PT* and *AT*) are not included for the gravity and wind loading cases (once designed for low-eccentricity conditions), because for these cases, the demands are much lower relative to capacities for all selected values of ϕ_{plate} and ϕ_{rod} (resulting in β values greater than 4.9 in all cases), thereby making their selection inconsequential. Referring to Figs. 6(a)-(e) for the remaining limit states, the following observations may be made:

- For the base plate, the *PC* limit state controls (in a vast majority of cases) over the *PT* limit state for the seismic loading cases, and is the only possible plate limit state for wind and gravity (that are designed for low-eccentricity conditions). Thus, focusing on the *PC* limit states across the three load cases (seismic, gravity, and wind) provides insights into suitable ϕ_{plate} – factors. Specifically, it is noted that: (1) the current estimate of ϕ_{plate} = 0.9 used in DG1, results in unacceptable median β values in the range of 1.9 – 3.2 for the three load cases, and (2) the value of ϕ_{plate} = 0.6 results in acceptable (median) β values, in the range of 4.1 – 5.1.
- For the *AT* limit state (which is shown only for the seismic load cases), a similar trend is observed, such that the current value (i.e., ϕ_{rod} = 0.75) results in β values in the range of 0.3 – 2.1 (unacceptable), whereas a value of ϕ_{rod} = 0.35 results in more acceptable values of β (with median = 3.6).

Since the suitable ϕ values for both the base plate and the anchor rods are significantly lower than those commonly used, this observation bears some explanation. Specifically, the current values of

ϕ_{plate} and ϕ_{rod} are directly adopted from the AISC Specification (AISC 2016a) for plate bending and axial tension in threaded rods. In turn, these values are calibrated based on reliability analysis in which demands (i.e., dead and/or live loads) with their associated distributions, are applied directly to the components. In contrast, for the ECBP connections, the demands (with similar distributions) are applied at the connection level rather than the component level. This distinction is important, because the component forces (e.g., $M_{pl,comp}$, $M_{pl,ten}$ or T_{rods}) are related to the connection demands (i.e., *P*-*M* pairs) in a highly nonlinear manner. Thus, the uncertainties in the component demands are greatly amplified relative to those at the connection level. A lower $\phi-$factor (applied to the capacity) is necessary to compensate for this effect, and produce an acceptable level of safety. Based on observations of Figs. 6(a)-(e) above, ϕ_{plate} = 0.6 and ϕ_{rod} = 0.35 are recommended as prospective $\phi-$factors for use with the DG1* approach. Fig. 7 shows histograms similar to those presented for the DG1 reliability analysis for these $\phi-$factors as applied to the DG1* method – these histograms illustrate expected β values for all limit states and load combinations. As expected, the histograms suggest that using the DG1* approach with these $\phi-$factors results in acceptable values of reliability across all limit states, and for all loadings.

Figs. 8(a)-(b) show the β versus ϕ plots for the CF approach (i.e., for connections designed only based on the *PT* and *AT* limit states). The *PT* and *AT* limit states are relevant only for the seismic cases, because only these cases result in the high-eccentricity condition. The observations from Figs. 8(a)-(b) are qualitatively similar to those noted previously for the DG1* approach. Specifically, the current values of ϕ_{plate} = 0.9, and ϕ_{rod} = 0.75 result in grossly unacceptable levels of reliability for both the *PT* and *AT* limit states. Based on the trends shown in these figures, the values of ϕ_{plate} = 0.4, and ϕ_{rod} = 0.35 are suggested for use with the CF approach. Fig. 9 shows the resulting β values for the three limit states (note that the *PC* limit state is omitted from the CF analysis). Referring to the figure, it is evident that these $\phi -$ factors, used within the CF approach result in acceptable values of β (> β_T = 3.6) across all limit states. It is interesting to observe that the ϕ_{plate} = 0.4 required to produce acceptable β values for the CF approach is lower than the corresponding ϕ_{plate} (= 0.6) for the DG1* approach, suggesting that the CF approach will result in a thicker base plate. However, this is not true, because the *PC* limit state, which is disregarded in the CF approach (but included in the DG1* approach), in fact results in significantly thicker base plates, in a large majority of cases.

To examine the implications for design more generally, Figs. 10(a)-(f) compare the plate thickness (t_p) as well as the anchor rod sizes generated by all three methods (i.e., DG1, DG1*, and CF) for each of the design cases. The first column of the figures (i.e., Figs. 10(a), (c), and (e)) illustrate the plate thicknesses (in all cases, ASTM A572 Grade 50 plate was specified), while the second column (Figs. 10(b), (d), and (f)) illustrate the anchor rod areas ($A_{\text{rods,all}}$). For the latter, ASTM F1554 Grade 55 steel was used in most cases except when congestion of anchor rods necessitated the use of a higher grade (i.e., Grade 105) for reducing the number/size of rods. The figures only report the rod area ($A_{\text{rods,all}}$). Referring to these figures, the following observations may be made:

- Figs. 10(a) and (b) compare the DG1 and DG1* approaches. The primary observation is that the DG1* approach results in thicker base plates as well larger anchor rods as compared to the DG1 approach. This is not surprising since the DG1 approach (owing to its use of the $\phi_{\text{bearing}} -$ factor in the equations to determine plate flexure and rod tension) unconservatively mischaracterizes the demands in these components. On average, the thickness of the plate as determined by DG1* is 1.28 times the thickness determined by DG1, whereas the rod area is 1.84 times the rod area determined by DG1 (for seismic design cases only).

- Figs. 10(c) and (d) compare the DG1 and CF approaches. The CF approach results in similar plate thicknesses as compared to the DG1 approach; this is not surprising, since the CF approach does not consider the *PC* limit state that controls in a majority of the design cases. On the other hand, the CF approach results in significantly larger anchor rod areas compared to DG1. This is similar to the comparison between DG1 and DG1* above, and may be attributed to: (1) the absence of the ϕ_{bearing} – factor in the CF approach, when estimating forces and moments in the anchor rods and the base plate, and (2) recalibration of the lower ϕ_{rod} – factor (= 0.35) in the CF approach to achieve acceptable reliability.
- Figs. 10(e) and (f) compare the two prospective approaches, i.e., DG1* and CF. These result in exactly the same anchor rod sizes, since the basis for estimation of anchor rod forces (i.e., no ϕ_{bearing} in the equations) as well as ϕ_{rod} (= 0.35) are identical between the two approaches. On the other hand, the base plate thicknesses as determined by the CF approach, are on average, 25% lower than those determined by the DG1* approach.

Based on the reliability analysis outlined earlier, both prospective approaches provide acceptable and consistent levels of reliability across all limit states and loading cases, as compared to the DG1 approach, which does not. Of these, the DG1* approach is likely to increase the cost of the ECBP connections, since it requires, on average, thicker base plates as well as larger anchor rods. On the other hand, the CF approach results in thinner base plates but larger anchor rods. Nonetheless, it does admit the possibility of base plate yielding on the compression side of the connection. Suitable approaches for design may be selected or developed based on these observations.

Summary and Conclusions

Exposed Column Base Plate (ECBP) connections are commonly constructed in SMRFs across the United States and beyond. Methods to estimate the strength of these connections and design them are well-documented in scientific literature, as well as in design guidelines – primarily, the American Institute of Steel Construction's *Design Guide One* (DG1 – Fisher and Kloiber 2006). While mechanistic aspects of the strength models have been studied extensively, the reliability provided by ECBP connections designed as per these approaches has received relatively less attention. Motivated by this, a detailed reliability analysis of the DG1 approach is conducted. The results indicate that DG1 approach results in unacceptable and inconsistent probabilities of failure of the connection, which is largely controlled by flexural failure of the base plate on the compression side of the connection. This is attributed to the $\phi_{\text{bearing}}-$factor, which artificially reduces the flexural demands on the base plate. Further, it is noted that: (1) the probabilities of failure are inconsistent across the four limit states, and (2) the seismic load cases result in lower reliability for all limit states as compared to the gravity and wind cases. In response to these problems identified in the DG1 approach, two alternative design methods are suggested. Both eliminate the $\phi_{\text{bearing}}-$factor in the bearing stress used for calculating flexural stresses in the base plate, whereas one considers overall connection failure, rather than the failure of individual components within it. Both these approaches provide adequate reliability.

While the study suggests significant improvements to the current method for designing ECBP connections, it has several limitations that must be considered in its interpretation and application. First, the models used in this study inherit all the limitations of the internal force distributions implied by the DG1 approach that may be inaccurate for low-eccentricity cases (Gomez et al. 2010; Kanvinde et al. 2013). Further, the DG1 approach is also inapplicable to ECBP connections subjected to biaxial bending or if the connection is overtopped with a slab on grade (Hanks and Richards 2019) as is sometimes the case. For biaxial bending, studies suggest using an empirical interaction equation to interpolate for angles of resultant moment that are not aligned with the major or minor axes (e.g., see Choi and Ohi 2005; Fasaee et al. 2018; Lee et al. 2008a; b). Second, the study considers a limited number of SMRF configurations – and these may bias the design cases (in terms of size, and configuration) relative to ECBP connections that differ significantly – e.g., those found in mezzanine columns (Kanvinde et al. 2015), or storage racks (Petrone et al. 2016). Third, the distributions of random variables to define various forms of uncertainty are based on limited data/engineering judgement (in some cases) and are considered uncorrelated. Notwithstanding these limitations, the study presents a critical analysis of current and prospective design approaches that may be used to more effectively design ECBP connections.

Data Availability Statement

Some or all data, models, or code that support the findings of this study are available from the corresponding author upon reasonable request.

Acknowledgments

The first author would like to acknowledge the financial support from China Scholarship Council (CSC, under Grant Number: 201608330227) and University College London (UCL) through a joint research scholarship for his PhD study. Support from the Pacific Earthquake Engineering Research Center is also gratefully acknowledged by the corresponding author.

References

ACI (American Concrete Institute). (2019). *Building Code Requirements for Structural Concrete and Commentary (ACI 318-19)*. American Concrete Institute, Farmington Hills, MI.

AISC (American Institute of Steel Construction). (1986). *Load and Resistance Factor Design Specification for Structural Steel Buildings*. American Institute of Steel Construction, Chicago, IL.

AISC (American Institute of Steel Construction). (2005). *Seismic Provisions for Structural Steel Buildings (ANSI/AISC 341-05)*. American Institute of Steel Construction, Chicago, IL.

AISC (American Institute of Steel Construction). (2016a). *Specification for Structural Steel Buildings (ANSI/AISC 360-16)*. American Institute of Steel Construction, Chicago, IL.

AISC (American Institute of Steel Construction). (2016b). *Seismic Provisions for Structural Steel Buildings (ANSI/AISC 341-16)*. American Institute of Steel Construction, Chicago, IL.

AISC (American Institute of Steel Construction). (2016c). *Code of Standard Practice for Steel Buildings and Bridges (ANSI/AISC 303-16)*. American Institute of Steel Construction, Chicago, IL.

AISC (American Institute of Steel Construction). (2018). *Seismic Design Manual, 3rd Edition*. American Institute of Steel Construction, Chicago, IL.

ASCE (American Society of Civil Engineers). (2006). *Minimum Design Loads for Buildings and Other Structures (ASCE/SEI 7-05)*. American Society of Civil Engineers, Reston, VA.

ASCE (American Society of Civil Engineers). (2016). *Minimum Design Loads for Buildings and Other Structures (ASCE/SEI 7-16)*. American Society of Civil Engineers, Reston, VA.

ASTM (American Society for Testing and Materials). (2018). *Standard Specification for Anchor Bolts, Steel, 36, 55, and 105-ksi Yield Strength (ASTM F1554-18)*. ASTM International, West Conshohocken, PA.

ASTM (American Society for Testing and Materials). (2019). *Standard Specification for General Requirements for Rolled Structural Steel Bars, Plates, Shapes, and Sheet Piling (ASTM A6/A6M-19)*. ASTM International, West Conshohocken, PA.

Aviram, A., Stojadinovic, B., and Kiureghian, A. Der. (2010). *Performance and Reliability of Exposed Column Base Plate Connections for Steel Moment-Resisting Frames.* PEER Report 2010/107. Pacific Earthquake Engineering Research Center, Berkeley, CA.

Choi, J., and Ohi, K. (2005). "Evaluation on interaction surface of plastic resistance for exposed-type steel column bases under biaxial bending." *Journal of Mechanical Science and Technology*, 19(3), 826–835.

Cornell, C. A. (1969). "A Probability-Based Structural Code." *ACI Journal Proceedings*, 66(12), 974–985.

Cui, Y., Nagae, T., and Nakashima, M. (2009). "Hysteretic Behavior and Strength Capacity of Shallowly Embedded Steel Column Bases." *Journal of Structural Engineering*, 135(10), 1231–1238.

Drake, R. M., and Elkin, S. J. (1999). "Beam-Column Base Plate Design--LRFD Method." *Engineering Journal*, 36(1), 29–38.

Ellingwood, B. R., Galambos, T., MacGregor, J., and Cornell, C. (1980). *Development of a probability based load criterion for American national standard A58 building code requirements for minimum design loads in buildings and other structures, Special Publication 577*. US Department of Commerce, National Bureau of Standards, Washington, D.C.

Ermopoulos, J. C., and Stamatopoulos, G. N. (1996). "Mathematical modelling of column base plate connections." *Journal of Constructional Steel Research*, 36(2), 79–100.

Fahmy, M. (2000). "Seismic Behavior of Moment-resisting Steel Column Bases." PhD Thesis. University of Michigan, Ann Arbor.

Falborski, T., Torres-Rodas, P., Zareian, F., and Kanvinde, A. (2020). "Effect of Base-Connection Strength and Ductility on the Seismic Performance of Steel Moment-Resisting Frames." *Journal of Structural Engineering*, 146(5), 04020054.

Fasaee, M. A. K., Banan, M. R., and Ghazizadeh, S. (2018). "Capacity of exposed column base connections subjected to uniaxial and biaxial bending moments." *Journal of Constructional Steel Research*, 148, 361–370.

Fayaz, J., and Zareian, F. (2019). "Reliability Analysis of Steel SMRF and SCBF Structures Considering the Vertical Component of Near-Fault Ground Motions." *Journal of Structural Engineering*, 145(7), 04019061.

Fisher, J. M., and Kloiber, L. A. (2006). *Design Guide 1: Base Plate and Anchor Rod Design (Second Edition)*. American Institute of Steel Construction, Chicago, IL.

Gomez, I., Kanvinde, A., and Deierlein, G. (2010). *Exposed Column Base Connections Subjected to Axial Compression and Flexure*. Chicago, IL.

Gomez, I. R. (2010). "Behavior and Design of Column Base Connections." PhD Thesis. University of California, Davis.

Gomez, I. R., Kanvinde, A. M., and Deierlein, G. G. (2011). "Experimental Investigation of Shear Transfer in Exposed Column Base Connections." *Engineering Journal*, 48(4), 245–264.

Grilli, D., Jones, R., and Kanvinde, A. (2017). "Seismic Performance of Embedded Column Base Connections Subjected to Axial and Lateral Loads." *Journal of Structural Engineering*, 143(5), 04017010.

Hanks, K. N., and Richards, P. W. (2019). "Experimental Performance of Block-Out Connections at the Base of Steel Moment Frames." *Journal of Structural Engineering*, 145(7), 04019057.

Hawkins, N. M. (1968). "The bearing strength of concrete loaded through rigid plates." *Magazine of Concrete Research*, 20(62), 31–40.

Iervolino, I., and Galasso, C. (2012). "Comparative assessment of load–resistance factor design of FRP-reinforced cross sections." *Construction and Building Materials*, 34, 151–161.

Kanvinde, A. M., Higgins, P., Cooke, R. J., Perez, J., and Higgins, J. (2015). "Column Base Connections for Hollow Steel Sections: Seismic Performance and Strength Models." *Journal of Structural Engineering*, 141(7), 04014171.

Kanvinde, A. M., Jordan, S. J., and Cooke, R. J. (2013). "Exposed column base plate connections in moment frames — Simulations and behavioral insights." *Journal of Constructional Steel Research*, 84, 82–93.

Lee, D.-Y., Geol, S. C., and Stojadinovic, B. (2008a). "Exposed Column-Base Plate Connections Bending About Weak Axis: I. Numerical Parametric Study." *International Journal of Steel Structures*, 8(1), 11–27.

Lee, D.-Y., Goel, S. C., and Stojadinovic, B. (2008b). "Exposed Column-Base Plate Connections Bending About Weak Axis: II. Experimental Study." *International Journal of Steel Structures*, 8(1), 29–41.

Liu, J., Sabelli, R., Brockenbrough, R. L., and Fraser, T. P. (2007). "Expected Yield Stress and Tensile Strength Ratios for Determination of Expected Member Capacity in the 2005 AISC Seismic Provisions." *Engineering Journal*, 44(1), 15–26.

Myers, A. T., Kanvinde, A. M., Deierlein, G. G., and Fell, B. V. (2009). "Effect of weld details on the ductility of steel column baseplate connections." *Journal of Constructional Steel Research*, 65(6), 1366–1373.

NEHRP (National Earthquake Hazards Reduction Program). (2010). *Evaluation of the FEMA P-695 Methodology for Quantification of Building Seismic Performance Factors, NIST GCR 10-917-8*. NEHRP Consultants Joint Venture.

Nowak, A. S., and Collins, K. R. (2012). *Reliability of Structures (2nd Edition)*. CRC Press, Taylor

& Francis Group, Boca Raton, FL.

Nowak, A. S., and Szerszen, M. M. (2003). "Calibration of Design Code for Buildings (ACI 318): Part 1—Statistical Models for Resistance." *ACI Structural Journal*, 100(3), 377-382.

OSHA (Occupational Safety and Health Administration). (2001). *Safety Standards for Steel Erection, (Subpart R of 29 CFR Part 1926)*. Occupational Safety and Health Administration, Washington, D.C.

Petrone, F., Higgins, P. S., Bissonnette, N. P., and Kanvinde, A. M. (2016). "The cross-aisle seismic performance of storage rack base connections." *Journal of Constructional Steel Research*, 122, 520–531.

Schmidt, B. J., and Bartlett, F. M. (2002). "Review of resistance factor for steel: data collection." *Canadian Journal of Civil Engineering*, 29(1), 98–108.

SEAOC (Structural Engineers Association of California). (2015). *2015 IBC SEAOC Structural/Seismic Design Manual Volume 1: Code Application Examples*. Structural Engineers Association of California, Sacramento, CA.

Torres-Rodas, P., Fayaz, J., and Zareian, F. (2020). "Strength resistance factors for seismic design of exposed based plate connections in special steel moment resisting frames." *Earthquake Spectra*, , 36(2), 537-553.

Torres-Rodas, P., Zareian, F., and Kanvinde, A. (2018). "Seismic Demands in Column Base Connections of Steel Moment Frames." *Earthquake Spectra*, 34(3), 1383–1403.

Trautner, C. A., Hutchinson, T., Grosser, P. R., and Silva, J. F. (2016). "Effects of Detailing on the Cyclic Behavior of Steel Baseplate Connections Designed to Promote Anchor Yielding." *Journal of Structural Engineering*, 142(2), 04015117.

Victorsson, V. K. (2011). "The reliability of capacity-designed components in seismic resistant systems." PhD Thesis. Stanford University.

Wald, F. (2000). "Column Base Modelling." *Semi-Rigid Joints in Structural Steelwork*, Springer Vienna, Vienna, 227–288.

Zareian, F., and Kanvinde, A. (2013). "Effect of Column-Base Flexibility on the Seismic Response and Safety of Steel Moment-Resisting Frames." *Earthquake Spectra*, 29(4), 1537–1559.

Table 1. Member sizes for 4-story archetype frames selected to generate *P*-*M* pairs for ECBP connection design

Story	RSA SDC-D_{max} frame			RSA SDC-D_{min} frame			ELF SDC-D_{max} frame			ELF SDC-D_{min} frame		
	Beam	Exterior column	Interior column	Beam	Exterior column	Interior column	Beam	Exterior column	Interior column	Beam	Exterior column	Interior column
1	W21×73	W24×103	W24×103	W16×57	W14×74	W14×82	W24×103	W24×103	W24×131	W18×71	W18×86	W18×97
2	W21×73	W24×103	W24×103	W18×60	W14×74	W14×82	W24×103	W24×103	W24×131	W18×86	W18×86	W18×97
3	W21×57	W24×62	W24×62	W18×60	W14×48	W14×74	W24×76	W24×76	W24×84	W18×71	W18×65	W18×86
4	W21×57	W24×62	W24×62	W16×57	W14×48	W14×74	W24×76	W24×76	W24×84	W18×71	W18×65	W18×86

Note: RSA = Response Spectrum Analysis; ELF = Equivalent Lateral Force; SDC = Seismic Design Category.

Table 2. Representative P-M matrix for ECBP connection design

Design case #	Frame	Base column	Site location[a]	Design load combination[b]		Base plate dimension[c]	
				P	M	N	B
1	RSA SDC-D$_{max}$	Exterior (W24×103)	LA	$1.2D + 0.5L - \Omega_0 E$	$1.1R_y M_p$	965 (38)	558 (22)
2				$1.2D + 0.5L + \Omega_0 E$	$1.1R_y M_p$		
3				$1.2D + 0.5L - W$	$1.2D + 0.5L - W$		
4				$1.2D + 0.5L + W$	$1.2D + 0.5L + W$		
5				$1.2D + 1.6L$	$1.2D + 1.6L$		
6 – 9			SAC	Same to cases 1 – 4[d]	Same to cases 1 – 4[d]		
10 – 14		Interior (W24×103)	LA[e]	Same to cases 1 – 5	Same to cases 1 – 5	965 (38)	558 (22)
15 – 19	RSA SDC-D$_{min}$	Exterior (W14×74)	LA	Same to cases 1 – 14	Same to cases 1 – 14	711 (28)	610 (24)
20 – 23			SAC				
24 – 28		Interior (W14×82)	LA			711 (28)	610 (24)
29 – 33	ELF SDC-D$_{max}$	Exterior (W24×103)	LA	Same to cases 1 – 14	Same to cases 1 – 14	965 (38)	558 (22)
34 – 37			SAC				
38 – 42		Interior (W24×131)	LA			965 (38)	660 (26)
43 – 47	ELF SDC-D$_{min}$	Exterior (W18×86)	LA	Same to cases 1 – 14	Same to cases 1 – 14	813 (32)	610 (24)
48 – 51			SAC				
52 – 56		Interior (W18×97)	LA			813 (32)	610 (24)
57 (SEAOC)[f]	–	W14×211	–	$(0.9\text{-}0.2S_{DS})D + \Omega_0 E$[f]	$(0.9\text{-}0.2S_{DS})D + \Omega_0 E$[f]	813 (32)	711 (28)
58 (DG1)[g]	–	W12×96	–	$1.2D + 1.6L$	$1.2D + 1.6L$	483 (19)	483 (19)
59 (DG1)[g]	–		–			508 (20)	508 (20)

[a]Two site locations in California are selected to reflect different seismic hazard levels for design: (1) LA = Los Angeles (high seismicity); (2) SAC = Sacramento (medium seismicity).

[b]The code specified D, L, W, and E loads are obtained from linear elastic analyses of archetype frames modeled in SAP2000.

[c]Two units are given for N and B: (1) Systéme International (SI) unit: mm; (2) U.S. customary unit in parentheses after the SI unit: in.

[d]The P-M pairs determined from gravity load combination for same base column at two locations are identical, therefore, only case 5 is considered.

[e]For interior column base, the seismic and wind loadings at two sites are similar, therefore, only the relatively larger values achieved from LA (owing high seismic hazard condition and higher basic wind speed) are considered to develop design cases.

[f]This case is employed from the design manual of Structural Engineers Association of California (SEAOC). This design example adopts different governing (seismic) load combinations, where, S_{DS} (= 1) is the assumed design (5% damped) spectral response acceleration parameter at short periods.

[g]These two cases are employed from the DG1 – case 58 is designed for low-eccentricity condition, while case 59 is designed for high-eccentricity condition.

Table 3. Summary of random variables (RVs) for reliability analysis of ECBP connections

Category	Variable	Bias	CoV (%)	Distribution
Geometry	Overall depth of base column section, d	0.999	0.2	Normal
	Flange width of base column section, b_f	0.998	0.4	Normal
	Flange thickness of base column section, t_f	1.04	2.5	Normal
	Web thickness of base column section, t_w	1.04	2.5	Normal
	Base plate length, N	1.0	2.5	Normal
	Base plate width, B	1.0	4	Normal
	Base plate thickness, t_p	1.0	3	Normal
	Anchor rod diameter, d_{rod}	1.0	8.5	Normal
	Edge distance, g	1.0	5	Normal
Material	Concrete compressive strength, $f_c^{'}$	1.235	14.5	Normal
	Grout compressive strength, f_{grout}	1.0	13	Normal
	Ratio of expected to specified minimum yield strength of W-shaped column steel (ASTM A992), R_y (nominal = 1.1)	1.0	5	Normal
	Yield strength of base plate steel, $F_{y,pl}$			
	ASTM A36	1.39	7	Normal
	ASTM A572 Grade 50	1.16	7	Normal
	Tensile (ultimate) strength of anchor rod steel, F_u			
	ASTM F1554 Grade 36	1.19	16	Lognormal
	ASTM F1554 Grade 55	1.13	12	Lognormal
	ASTM F1554 Grade 105	1.1	9	Lognormal
Load	Dead load, D	1.05	10	Normal
	Live load, L	1.0	25	Gumbel
	Wind load, W	0.78	37	Gumbel
	Earthquake load, E	1.0	60	Lognormal
Model	Ratio of concrete bearing stress to concrete compressive strength, $f_{\text{concrete}}^{\text{test}} / f_{\text{concrete}}^{\text{Eq.(2)}}$	1.07	16	Normal
	Error in characterization of flexural demand of base plate on the compression side, $M_{pl,comp}^{\text{true}} / M_{pl,comp}^{\text{model}}$			
	DG1 model	0.88	19	Normal
	DG1* and CF models	0.74	20	Normal
	Error in characterization of flexural demand of base plate on the tension side, $M_{pl,ten}^{\text{true}} / M_{pl,ten}^{\text{model}}$			
	DG1 model	0.99	12	Normal
	DG1* and CF models	1.1	14	Normal
	Error in Characterization of tension demand in anchor rods, $T_{\text{rods}}^{\text{true}} / T_{\text{rods}}^{\text{model}}$			
	DG1 model	0.99	12	Normal
	DG1* and CF models	1.1	14	Normal

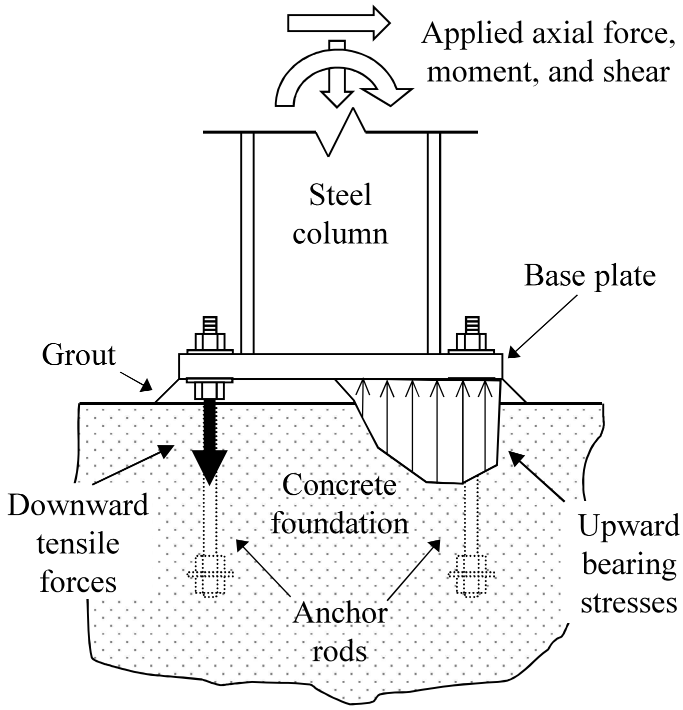

Fig. 1. Schematic illustration of an exposed column base plate (ECBP) connection and force transfer mechanisms

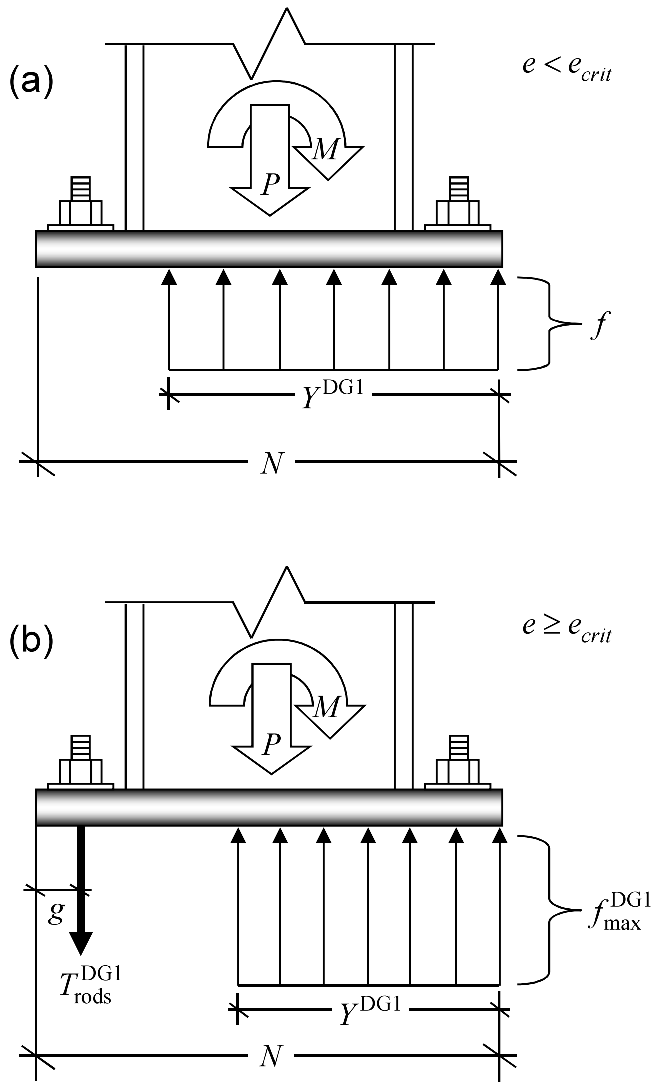

Fig. 2. Internal stress distributions used in the *Design Guide One* (DG1) method: (a) low-eccentricity and (b) high-eccentricity conditions

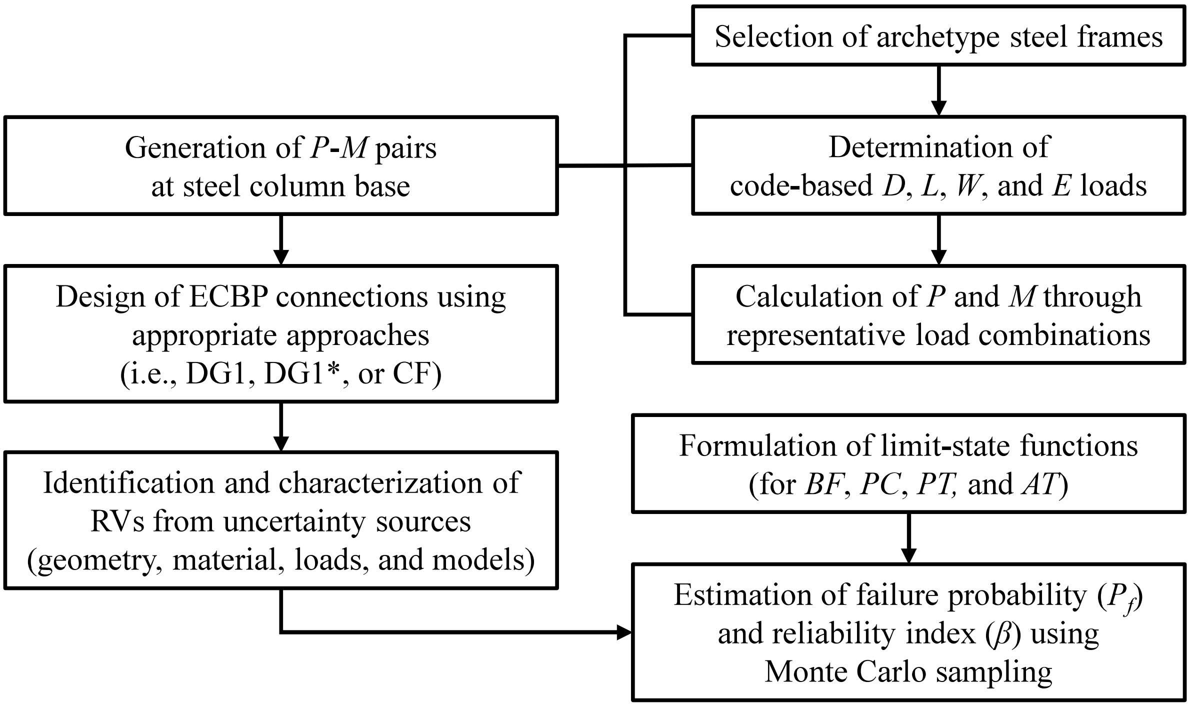

Fig. 3. Flowchart of the methodology for reliability assessment of ECBP connections designed as per current and prospective approaches

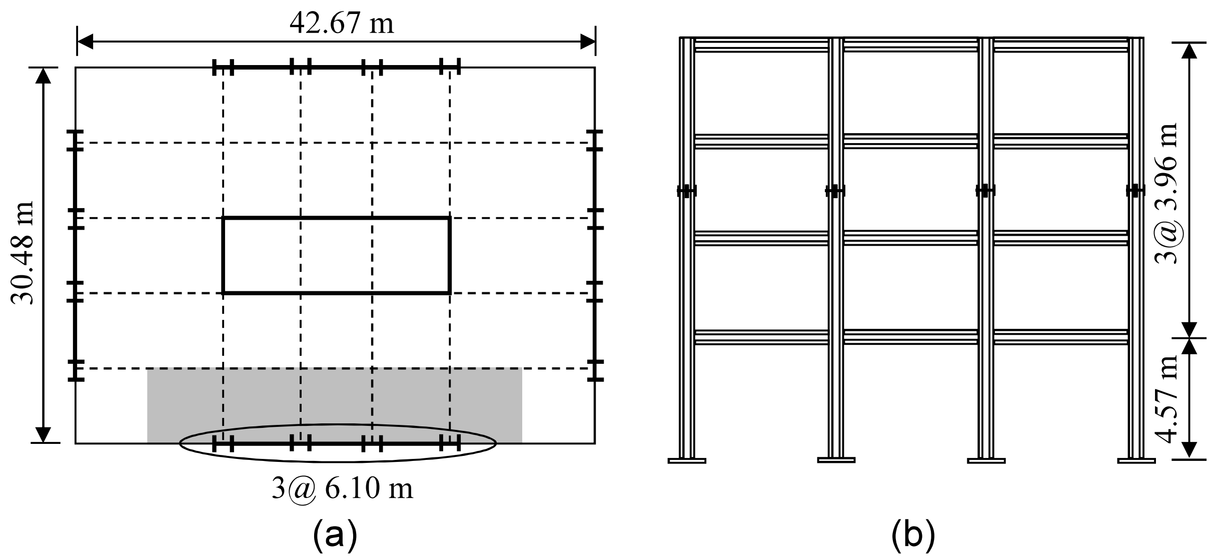

Fig. 4. Schematic illustration of 4-story archetype frames: (a) plan configuration; and (b) elevation view

Figure 5 Click here to access/download;Figure;Fig5.pdf

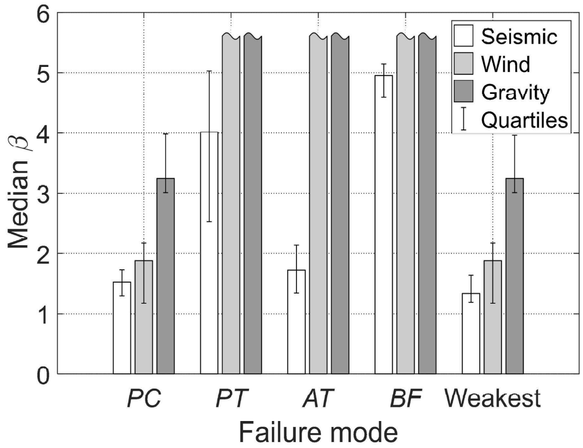

Fig. 5. Median reliability index (β) values (with respect to different failure modes and load combinations) of ECBP connections designed as per the DG1 method

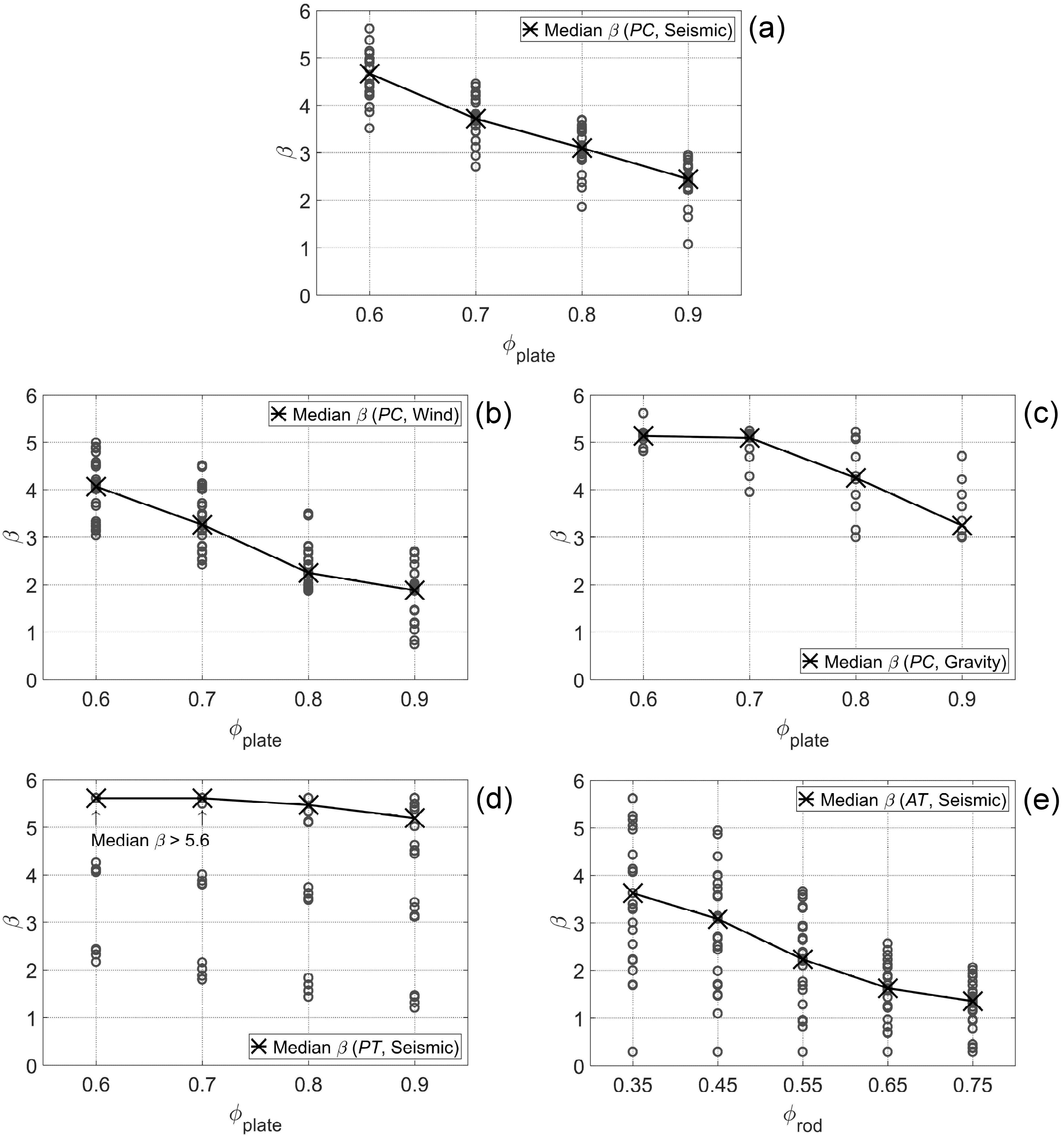

Fig. 6. Reliability index (β) plotted against trial ϕ–factors for the DG1* approach: β vs. ϕ_{plate} for *PC* check considering (a) seismic, (b) wind, and (c) gravity load cases, respectively; (d) β vs. ϕ_{plate} for *PT* check and (e) β vs. ϕ_{rod} for *AT* check, both only considering seismic load cases

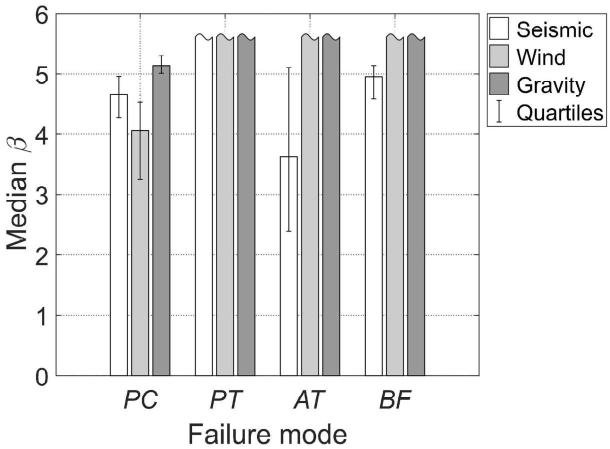

Fig. 7. Median reliability index (β) values (with respect to different failure modes and load combinations) of ECBP connections designed as per the DG1* method.

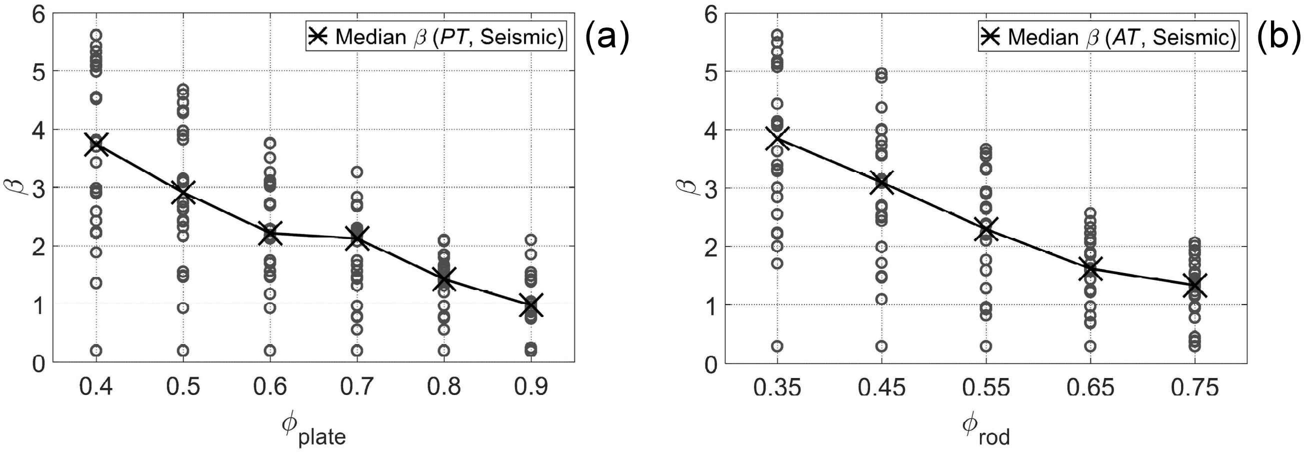

Fig. 8. Reliability index (β) plotted against trial ϕ–factors for the CF approach: (a) β vs. ϕ_{plate} for *PT* limit-state check and (b) β vs. ϕ_{rod} for *AT* limit-state check, for seismic load cases

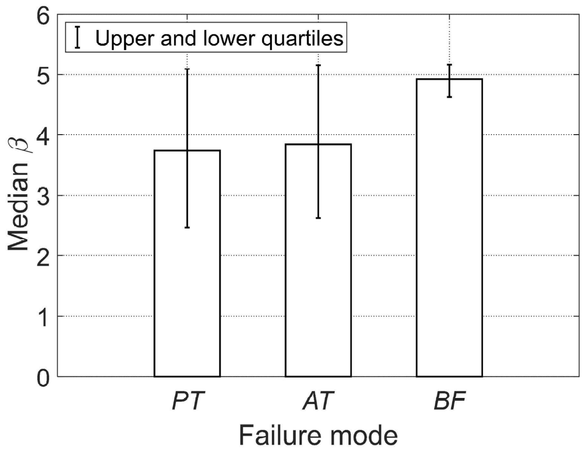

Fig. 9. Median reliability index (β) values (with respect to different failure modes and seismic load combinations) of ECBP connections designed as per the CF method

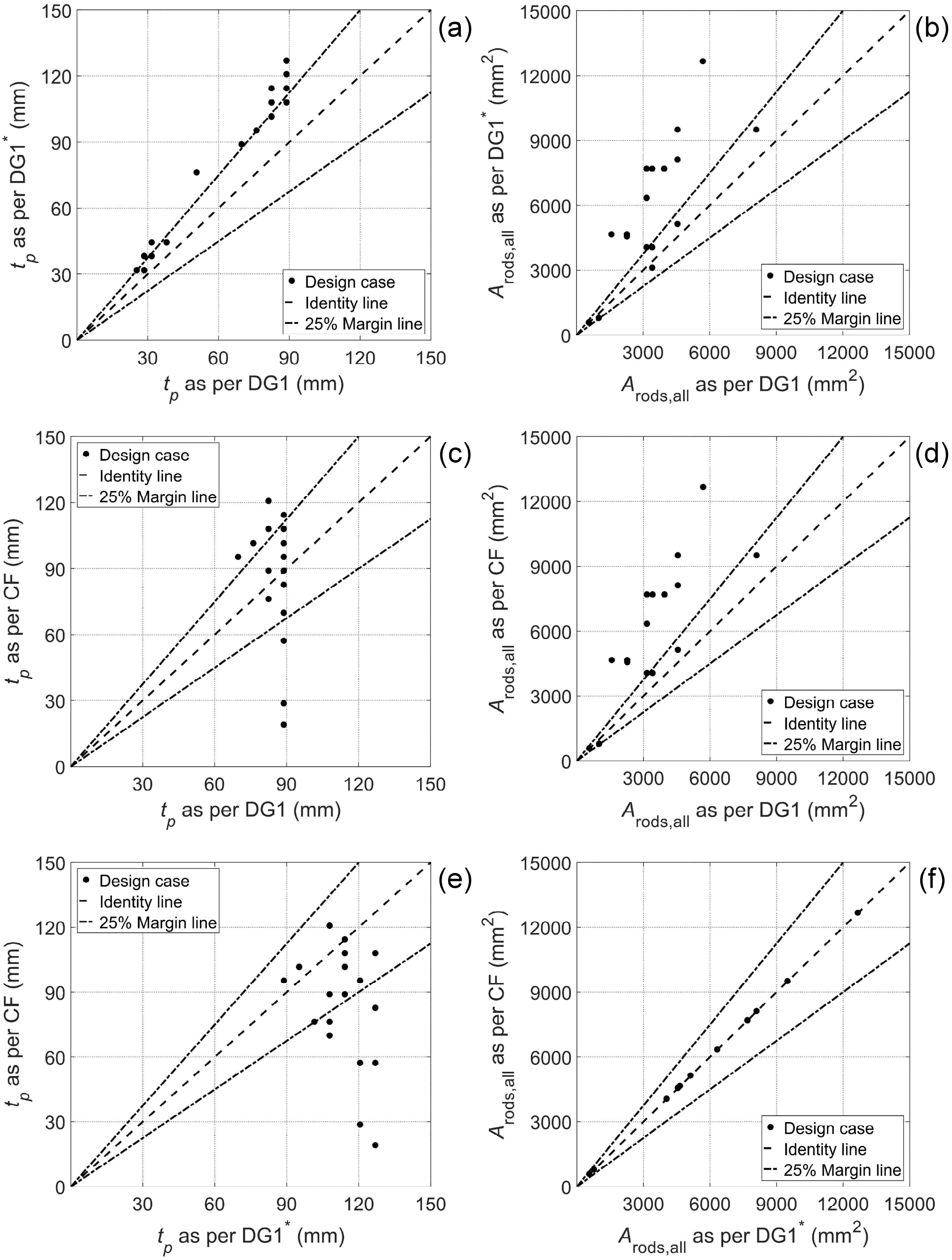

Fig. 10. Comparisons of plate thickness (t_p) and total anchor rod area ($A_{rods,all}$) for ECBP connections designed as per the DG1, DG1* and CF methods.

Fig. 1. Schematic illustration of an exposed column base plate (ECBP) connection and force transfer mechanisms

Fig. 2. Internal stress distributions used in the *Design Guide One* (DG1) method: (a) low-eccentricity and (b) high-eccentricity conditions

Fig. 3. Flowchart of the methodology for reliability assessment of ECBP connections designed as per current and prospective approaches

Fig. 4. Schematic illustration of 4-story archetype frames: (a) plan configuration; and (b) elevation view

Fig. 5. Median reliability index (β) values (with respect to different failure modes and load combinations) of ECBP connections designed as per the DG1 method

Fig. 6. Reliability index (β) plotted against trial ϕ–factors for the DG1* approach: β vs. ϕ_{plate} for *PC* check considering (a) seismic, (b) wind, and (c) gravity load cases, respectively; (d) β vs. ϕ_{plate} for *PT* check and (e) β vs. ϕ_{rod} for *AT* check, both only considering seismic load cases

Fig. 7. Median reliability index (β) values (with respect to different failure modes and load combinations) of ECBP connections designed as per the DG1* method

Fig. 8. Reliability index (β) plotted against trial ϕ–factors for the CF approach: (a) β vs. ϕ_{plate} for *PT* limit-state check and (b) β vs. ϕ_{rod} for *AT* limit-state check, for seismic load cases

Fig. 9. Median reliability index (β) values (with respect to different failure modes and seismic load combinations) of ECBP connections designed as per the CF method

Fig. 10. Comparisons of plate thickness (t_p) and total anchor rod area ($A_{\mathrm{rods,all}}$) for ECBP connections designed as per the DG1, DG1* and CF methods